Geophysical Research Letters

RESEARCH LETTER
10.1029/2024GL111402

Field Observations of Surfzone Vorticity

C. Dooley[1,2], Steve Elgar[1], and Britt Raubenheimer[1]

[1]Woods Hole Oceanographic Institution, Woods Hole, MA, USA, [2]Massachusetts Institute of Technology, Cambridge, MA, USA

Key Points:

- Surfzone vorticity is estimated for the first time with unique field observations within, across, and along the surfzone
- In situ observations show that small-scale vorticity injected by breaking waves increases with wave directional spread
- Remotely sensed observations show large-spatial scale vorticity increases as bathymetry becomes more alongshore inhomogeneous

Correspondence to:
C. Dooley,
cdooley@whoi.edu

Citation:
Dooley, C., Elgar, S., & Raubenheimer, B. (2024). Field observations of surfzone vorticity. *Geophysical Research Letters*, *51*, e2024GL111402. https://doi.org/10.1029/2024GL111402

Received 15 JUL 2024
Accepted 26 SEP 2024

Abstract In the surfzone, breaking-wave generated eddies and vortices transport material along the coast and offshore to the continental shelf, providing a pathway from land to the ocean. Here, surfzone vorticity is investigated with unique field observations obtained during a wide range of wave and bathymetric conditions on an Atlantic Ocean beach. Small spatial-scale [O(10 m)] vorticity estimated with a 5 m diameter ring of 14 current meters deployed in ∼2 m water depth increased as the directional spread of the wave field increased. Large spatial-scale [O(100 m)] vorticity calculated from remote sensing estimates of currents across the surfzone along 200 m of the shoreline increased as alongshore bathymetric variability (channels, bars, bumps, holes) increased. For all bathymetric conditions, large-scale vorticity in the inner surfzone was more energetic than in the outer surfzone.

Plain Language Summary Circular, rotating flow features, such as eddies, swirls, and vortices mix and disperse material throughout the ocean. Here, circular flow features that can transport sediments, pollutants, and biota from the shore to the continental shelf were investigated using field observations from a 5 m diameter ring of current meters in 2 m depth and from tracking naturally occurring ocean foam visible in optical images of the surfzone (where waves break) spanning 200 m of the coast. The observations show that small-scale flow patterns become more energetic as ocean waves arrive from a wider range of directions and that large-scale flow features become more energetic as the seafloor becomes more nonuniform (including holes and channels).

1. Introduction

In the shallow surfzone, waves shoal and break along the coast, generating eddies and vortices that contribute to mixing and dispersion, and transport materials from the shoreline to the inner continental shelf, and along the coast (Brown et al., 2019; Clark et al., 2010; Feddersen, 2007; Feddersen et al., 2011; Hally-Rosendahl & Feddersen, 2016; Hally-Rosendahl et al., 2014, 2015; and others). These processes affect the distribution of bacteria, larvae, pollutants, and sediment (Boehm, 2003; Feddersen et al., 2021; Grant et al., 2005), and thus are important to human (Boehm et al., 2017; Moulton et al., 2023) and ecosystem health (Morgan et al., 2018). Determining how surfzone vorticity is generated and evolves is necessary for understanding, and thus modeling, the fundamental physics of circulation in the nearshore coastal ocean.

In the shallow waters of the surfzone short-crested breaking waves ($0.05 < f < 0.25$ Hz, where f is frequency) have been hypothesized (Bühler, 2000; Peregrine, 1998, 1999) to be a source of small [O(10 m)] length-scale eddies. Specifically, the wave breaking-induced change in vertical vorticity $\Delta\omega_d$ is (Peregrine, 1999):

$$\Delta\omega_d = \left[\frac{2h_2}{gh_1(h_1+h_2)}\right]^{1/2}\frac{dE_d}{dy_c}, \tag{1}$$

where h_1 and h_2 are the instantaneous water depths in front of and behind the breaking wave, respectively, E_d is the breaking dissipation, and y_c is the distance in the along-crest direction. The along-crest change in dissipation (dE_d/dy_c) is greatest at the end of a breaking wave (crest end) where there are adjacent regions of breaking and non-breaking (Figure 1). Numerical simulations also suggest that short-crested breaking waves can generate vorticity, and that vorticity variance and dispersion increase with the number of crest ends (via directional spread) (Baker et al., 2021; Bonneton et al., 2010; Bruneau et al., 2011; Bühler, 2000; Bühler & Jacobson, 2001; Geiman & Kirby, 2013; Johnson & Pattiaratchi, 2006; O'Dea et al., 2021; Spydell et al., 2009; Wei et al., 2017).

Recent numerical model studies have investigated vorticity in the surfzone, with emphasis on the roles of breaking waves and the underlying bathymetry. Field data to validate results are limited, in part due to the

© 2024. The Author(s).
This is an open access article under the terms of the Creative Commons Attribution-NonCommercial-NoDerivs License, which permits use and distribution in any medium, provided the original work is properly cited, the use is non-commercial and no modifications or adaptations are made.

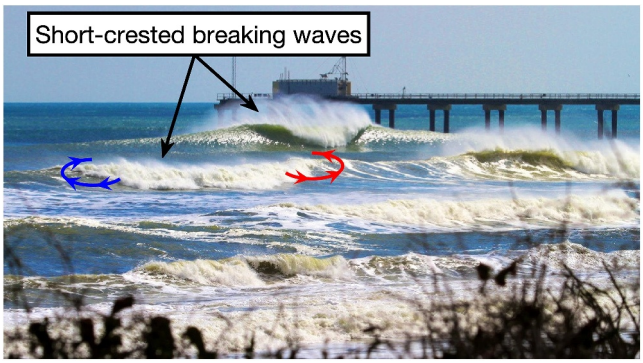

Figure 1. Photograph of short-crested [O(10 m) length scales] waves breaking in the surfzone that generate rotational forcing that injects negative (blue) and positive (red) vorticity into the water column.

challenge of deploying and maintaining in situ instrumentation in the surfzone, and the limited spatial resolution of measurements. Phase-resolving wave models that simulate currents and vorticity on idealized bathymetry (Baker et al., 2021; O'Dea et al., 2021) suggest that the energy of small-spatial scale [O(10 m)] surfzone vorticity increases with increasing directional spread of the wave field (more injection due to short crested breaking), and that larger-scale [O(100 m)] vorticity (rip currents and circulation cells) increases as the variability of the bathymetry increases (Baker et al., 2021; Kennedy et al., 2006; O'Dea et al., 2021).

Here, during a wide range of incident wave conditions, small spatial-scale [O(10 m)] vorticity in the surfzone was estimated (Clark et al., 2012) with a unique 5 m diameter ring of current meters, allowing comparison with the corresponding statistics of the wave field, in particular the spread in directions from which waves arrive. In addition, large spatial-scale [O(100 m)] vorticity was estimated from remotely sensed currents every 3.2 m across the surfzone along 200 m of the shoreline, allowing the effects of bathymetric variability to be investigated with field observations for the first time.

2. Observations

In 2013, a 5 m diameter ring of 14 current meters was deployed in ~2.0 to 2.5 m water depth in the surfzone (Figure 2) for 29 days to measure mean vertical vorticity at the U.S. Army Corps of Engineers Field Research Facility (FRF) on the Atlantic Ocean in Duck, NC. The current meters were sampled at 8 Hz, resolving vorticity injection by individual waves. Vertical vorticity within the ring of current meters (Figure 2) was estimated using Kelvin's circulation theorem $\overline{\omega} = A^{-1} \oint u \cdot dl$, where A is the area inside the array, u is the horizontal velocity vector estimated from the current meters, and l is the closed path around the perimeter of the array (Clark et al., 2012; Thomson, 1910). Vorticity averages and variances were considered across 60 min periods.

Remotely sensed imagery for estimating surface currents was collected during daytime hours using optical cameras mounted on a ~40 m tall tower overlooking the surfzone. Nearshore flows were estimated from the imagery using naturally occurring foam as a tracer for surface currents and the Particle Image Velocimetry (PIV) algorithm (Dooley, Elgar, Raubenheimer, & Gorrell, 2024 and references therein), resulting in 2 min mean flow estimates every 3.2 × 3.2 m across the surfzone (Figure 3). Vorticity $\overline{\omega}$ was estimated from this flow field from the curl of the velocity ($\overline{\omega} = \nabla \times \overrightarrow{u}$), where the partial derivatives of the velocity are estimated using finite differences (color contours, Figures 3a and 3c). To reduce errors in velocity estimates that can increase with distance from the camera and obliqueness of the viewing angle (Dooley, Elgar, Raubenheimer, & Gorrell, 2024), only the 200 m of coastline closest to the camera were analyzed. Data were collected in 2013 during the ring deployment

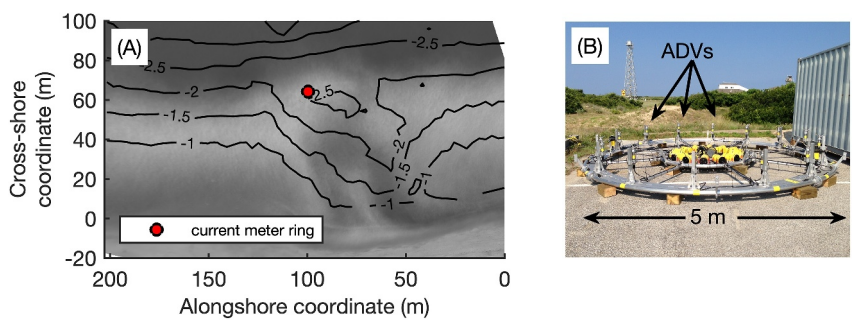

Figure 2. (a) Bathymetry (contour curves every 0.5 m) on 1 October 2013 as a function of cross- and alongshore coordinates at the USACE Field Research Facility, Duck, NC. The coordinate system originates at the shoreline and the edge of the camera field of view. The grayscale background is a 10 min time-averaged image of the surfzone, where lighter areas indicate foam caused by breaking waves. The current meter ring is indicated by the red circle. (b) Current meter ring before deployment by helicopter into the surfzone (3 of the 14 Acoustic Doppler Velocimeters (ADVs) are indicated by the arrows).

19448007, 2024, 20, Downloaded from https://agupubs.onlinelibrary.wiley.com/doi/10.1029/2024GL111402 by Ciara Dooley - Mbl Whoi Library , Wiley Online Library on [24/10/2024]. See the Terms and Conditions (https://onlinelibrary.wiley.com/terms-and-conditions) on Wiley Online Library for rules of use; OA articles are governed by the applicable Creative Commons License

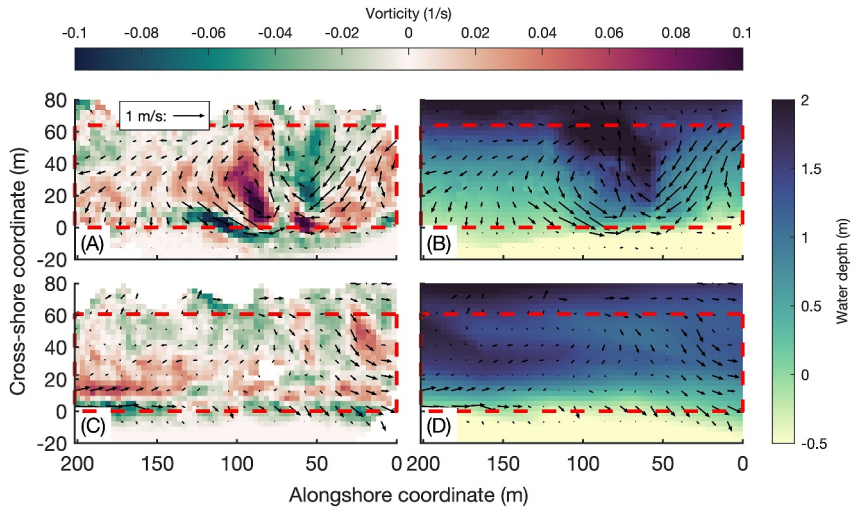

Figure 3. Remotely sensed estimates of 2 min mean surface currents (arrows point in the direction of flow with length proportional to speed, only every third vector is shown) as a function of cross-and alongshore coordinates for high bathymetric variability on 1 October 2013 (a), (b) and low bathymetric variability on 29 August 2021 (c), (d). Currents are superimposed on color contours of vorticity (scale on top) (a), (c) and bathymetry (scale on right) (b), (d). The red dashed lines enclose the surfzone. The current meter ring was located at cross- and alongshore coordinates 60 and 100 m during the 2013 experiment (Figure 2).

(Elgar et al., 2023; Elgar & Raubenheimer, 2020), and during 2018, 2021 (Chen et al., 2024; Salatin et al., 2024; Straub et al., 2023), and 2022 (Dooley, Elgar, Raubenheimer, & Gorrell, 2024) across varying bathymetries.

Mean hourly vorticity estimated at the current meter ring is correlated with the vorticity estimated using remote sensing with $r^2 = 0.6$ ($n = 117$ points). The largest differences occur when strong offshore flows (undertow) were measured at the current meter ring (~2 m depth), consistent with variations between surface currents and mid-water column flows. For 2 min mean vorticity, results are less correlated, likely owing to noise in remote sensing estimates at short length and time scales. Incident conditions measured at the ring concurrent with remote sensing periods (daylight hours with sufficient foam to track at the ring) included significant wave heights that ranged from 0.5 to 1.5 m, centroidal frequencies that ranged from 0.12 to 0.18 Hz, and directions that ranged from −3° to +30° relative to shore normal with spreads from 12° to 24°.

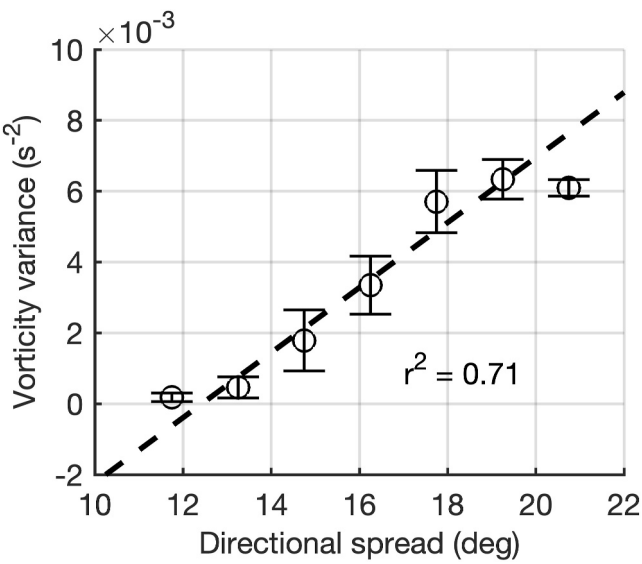

Figure 4. Vorticity variance versus wave directional spread estimated at the current meter ring at 8 Hz for 1 hr periods. Points are averaged into bins (8–38 points) where the circles indicate the mean value within each bin and the vertical bars are one standard deviation. The black dashed line corresponds to the best linear fit of the un-binned data, with $r^2 = 0.71$ ($n = 168$).

Bathymetry was measured intermittently, when wave conditions permitted, throughout each experiment using survey vehicles along cross-shore transects separated by ~45 m in the alongshore, with one survey in 2013 at ~13 m resolution (Figure 2a). To examine the relationship between bathymetric inhomogeneity and observed vorticity, remotely sensed flow estimates were considered for imagery collected within 1 day of a bathymetry survey. In addition, data were filtered to remove instances of insufficient foam coverage (e.g., large gaps in tracer between the shoreline and the edge of breakers). The contrasting requirements for remote sensing (larger waves generating adequate foam tracer) and bathymetric surveying (smaller waves safe for human transit) results in a dataset of 7 days. The observations include a range of bathymetries, varying from highly alongshore inhomogeneous (Figure 3b) with channels, crescentic sandbars, bumps, and holes to relatively alongshore uniform (Figure 3d).

Observed circulation patterns (Figure 3) often persisted for many days, modulating with the tide and incident wave conditions. Major changes in the strength and patterns of the currents occurred after storms with large incident waves (>3 m) that drove strong alongshore currents (>1 m/s), causing significant changes to the underlying bathymetry.

19448007, 2024, 20, Downloaded from https://agupubs.onlinelibrary.wiley.com/doi/10.1029/2024GL111402 by Ciara Dooley - Mbl Whoi Library , Wiley Online Library on [24/10/2024]. See the Terms and Conditions (https://onlinelibrary.wiley.com/terms-and-conditions) on Wiley Online Library for rules of use; OA articles are governed by the applicable Creative Commons License

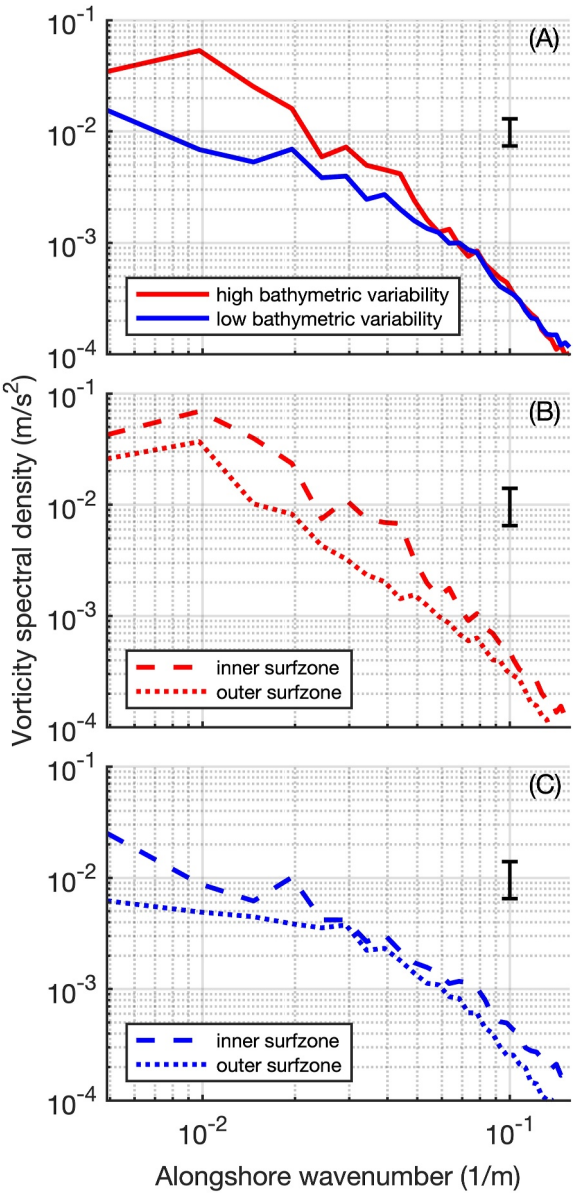

Figure 5. Spectral density of vorticity versus alongshore wavenumber for (a) high bathymetric variability (red curve, bathymetry in Figure 3b) on 1 October 2013 and low bathymetric variability (blue curve, bathymetry in Figure 3d) on 29 August 2021, (b) the inner (red dashed curve) and outer (red dotted curve) surfzone with high bathymetric variability on 1 October 2013, and (c) the inner (blue dashed curve) and outer (blue dotted curve) surfzone with low bathymetric variability on 29 August 2021. 95% confidence levels for (conservatively) 100 (a) and 50 (b), (c) degrees of freedom are indicated by the vertical bars (2 min spectra at each alongshore row, averaged over an hour (30 estimates) and the width of the full, inner, or outer surfzone (19 (a) alongshore rows or 9–10 (b), (c) alongshore rows)).

3. Results

The variation in vorticity was estimated at the current meter ring at 8 Hz for a period of 7 days during which the directional spread measured at the ring varied between 11° and 22° and there was sufficient breaking for the current meter ring to remain within the surfzone across tidal cycles. Significant wave heights at the ring ranged from 0.5 to 1.3 m, centroidal frequencies ranged from 0.11 to 0.16 Hz, and directions ranged from ±6° relative to shore normal. Bathymetric conditions were complex (Figure 2a), with corresponding complex large-scale circulation patterns (Figures 3a and 3b). The variance of vorticity estimated at the current meter ring increases with increasing directional spread (Figure 4, $r^2 = 0.7$), suggesting that small length-scale vorticity is injected into the water column by short-crested breaking waves, consistent with previous numerical simulations for somewhat limited and ideal conditions (Baker et al., 2021; Bonneton et al., 2010; Bruneau et al., 2011; Bühler, 2000; Bühler & Jacobson, 2001; Johnson & Pattiaratchi, 2006; O'Dea et al., 2021; Spydell et al., 2009). Vorticity variance was uncorrelated with other incident wave characteristics, including significant wave height. For the same period of wave conditions, but reduced to when remote sensing estimates were available (43 hr), the variance in 2 min mean vorticity estimated at the ring increases with increasing directional spread with $r^2 = 0.4$, whereas the vorticity estimated using remote sensing is uncorrelated with spread with $r^2 = 0.1$, suggesting the accuracy and resolution of remotely sensed estimates used here may not be sufficient to resolve injection by 8–10 s short-crested breaking waves.

To investigate if large-spatial scale vorticity is related to inhomogeneities in the bathymetry (Baker et al., 2021; O'Dea et al., 2021), vorticity at larger spatial scales was estimated from the remotely sensed currents that spanned the surfzone along 200 m of the shoreline (Figure 3). The alongshore wavenumber spectra of 2 min mean vorticity were calculated for alongshore transects (every 3.2 m) from the shoreline to the breakers, temporally averaged over an hour, and spatially averaged across the inner 50%, the outer 50%, and the full surfzone (Figure 5). Vorticity spectral energy at long wavelengths is higher for strongly alongshore varying bathymetry (Figures 3b and 5a) than it is for smoother bathymetry (Figures 3d and 5a). For cases of both high (Figures 3b and 5b) and low (Figures 3d and 5c) bathymetric variability the inner surfzone vorticity (dashed curves in Figures 5b and 5c) is more energetic than the vorticity estimated in the outer surfzone (dotted curves in Figures 5b and 5c), consistent with model results for narrower ranges of bathymetric variability (Baker et al., 2021; O'Dea et al., 2021).

Across the six measured bathymetries, vorticity variance (the area under the alongshore wavenumber spectra of vorticity) at long length scales ($L > 100$ m) is correlated ($r^2 = 0.8$) with alongshore bathymetric variance (Figure 6), suggesting O(100 m) nearshore vorticity is dominated by waves and currents interacting with bathymetric features. Bathymetric variance was evaluated as either the mean value of the variance of the measured alongshore bathymetry averaged over alongshore rows spaced every 3.2 m in the cross-shore spanning the surfzone (Figure 6) or as the area under the alongshore wavenumber spectra of bathymetry, with similar results ($r^2 = 0.8$, spectra of bathymetry were averaged over ~19 alongshore rows to provide ~38 degrees of freedom). Bathymetric and vorticity variance changes during observations corresponding to a single bathymetric survey because the domain of analysis fluctuates with changing tidal water levels and the associated surfzone widths. Some variation occurred within the 2 min mean spectra included in each 60 min averaging period (standard deviation bars, Figure 6), with the highest variation occurring for observations with the most inhomogeneous bathymetry.

19448007, 2024, 20, Downloaded from https://agupubs.onlinelibrary.wiley.com/doi/10.1029/2024GL111402 by Ciara Dooley - Mbl Whoi Library , Wiley Online Library on [24/10/2024]. See the Terms and Conditions (https://onlinelibrary.wiley.com/terms-and-conditions) on Wiley Online Library for rules of use; OA articles are governed by the applicable Creative Commons License

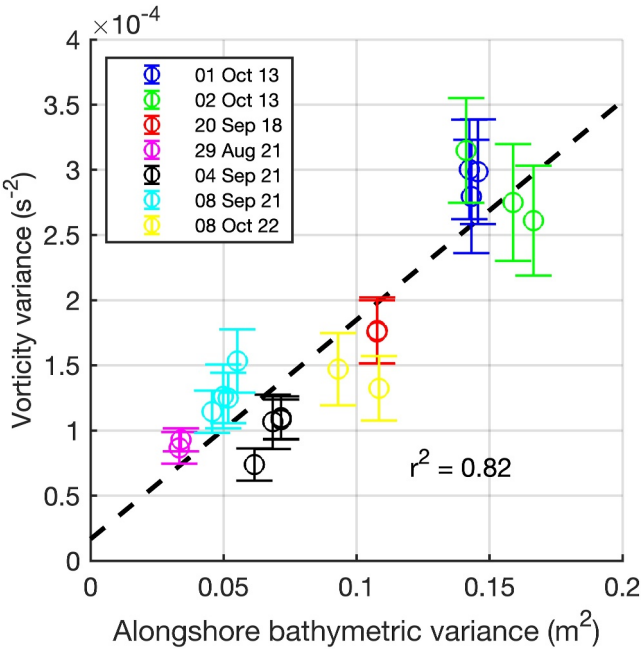

Figure 6. Vorticity variance at long length scales ($L > 100$ m) versus alongshore bathymetric variance for observations across different bathymetries (different colors correspond to different days, given in the legend), with vertical bars the standard deviation of the 2 min means in each 60 min average (circles). The black dashed line corresponds to the best linear fit, with $r^2 = 0.82$.

Incident wave conditions measured in 17 m water depth during these remote sensing observations included significant wave heights that ranged from 0.5 to 1.7 m, centroidal frequencies that ranged from 0.07 to 0.20 Hz, and directions that ranged from ±46° relative to shore normal with spreads from 22° to 35°. Incident wave, tidal, and mean cross- and alongshore flow conditions were uncorrelated with the variance of long length scale vorticity, suggesting that bathymetric features are the primary source of variability under these conditions.

4. Discussion

The results presented here include the first field estimates of surfzone vorticity, which demonstrate that both increasing wave directional spread and alongshore bathymetric variability can increase vorticity, and that vorticity can vary across the inner and outer surfzone. Vorticity is ubiquitous in the surfzone, and while wave-averaged numerical models can simulate some impacts of bathymetric variability on vorticity (Dalrymple et al., 2011; Haas et al., 2003, and others), new parameterizations or time-domain models are needed to simulate the effects of directionally spread wave breaking on vorticity generation.

Processes that may affect vorticity in the surfzone remain uncertain, including interactions between bathymetric and short-crested forced vorticity, vorticity generation by bathymetry and short-crested breaking with overlapping length scales, and the evolution of the coupled hydrodynamic-morphologic system from uniform flow and bathymetry to eddies and alongshore variable morphology. For example, breaking-wave-induced small-spatial scale vorticity can participate in a two-dimensional inverse energy cascade that transfers energy to larger-scale rotational motions (Baker et al., 2023; Elgar et al., 2023; Elgar & Raubenheimer, 2020; Spydell & Feddersen, 2009), and thus scales of vorticity forced by directionally spread waves may overlap with those owing to variable bathymetry. It is uncertain whether interaction of vorticity at these scales will result in more surfzone mixing, dispersion, and transport.

Obtaining spatially dense field estimates of vorticity to address these topics requires novel methods, such as the in situ current meter ring, the optical remote sensing used here, and other remote sensing techniques including radar and infrared sensing. Future applications of these techniques may improve the understanding of both the dynamics of the surfzone and interactions with shelf processes. Preliminary examination of the observed temporal changes of vorticity suggests that some complex circulation patterns may remain nearly stationary (perhaps tied to bathymetric features), whereas others may move (not shown). Thus, it also is important for future studies to examine the evolution and transient features of vorticity. For example, surfzone vortices can form dipoles that episodically are ejected offshore, forming concentrated flows (transient rip currents) extending seaward of the surfzone to the shelf (Grimes & Feddersen, 2021; Kumar & Feddersen, 2017; Suanda & Feddersen, 2015; Wu et al., 2021). These vorticity-generated flows could be an important mechanism for exchange between the surfzone and the inner shelf and can cause baroclinic circulation cells that extend into stratified deeper water (Grimes & Feddersen, 2021; Kumar & Feddersen, 2017). The observational methods presented here may enable studies of the combined effects of changing bathymetry and incident waves on transient rips. Continued observation of surfzone vorticity at a diversity of field sites would provide new data to further the understanding of nearshore dynamics.

5. Conclusions

Field observations of vorticity in the surfzone were investigated for a wide range of incident wave fields and nearshore bathymetries that varied from relatively alongshore homogeneous to strongly inhomogeneous with channels, crescentic sandbars, bumps, and holes. Small-scale [O(10 m)] vorticity estimated with Kelvin's circulation theorem and measurements from 14 current meters evenly spaced around a 5 m diameter ring deployed in ~2 m water depth increased with the directional spread of the wave field. Large-scale [O(100 m)] vorticity

19448007, 2024, 20, Downloaded from https://agupubs.onlinelibrary.wiley.com/doi/10.1029/2024GL111402 by Ciara Dooley - Mbl Whoi Library , Wiley Online Library on [24/10/2024]. See the Terms and Conditions (https://onlinelibrary.wiley.com/terms-and-conditions) on Wiley Online Library for rules of use; OA articles are governed by the applicable Creative Commons License

estimated from the curl of remotely sensed currents every 3.2 m across the surfzone along 200 m of the shoreline increased as the bathymetric variability increased, and the energy of the inner surfzone vorticity was greater than that in the outer surfzone. The results here help determine how surfzone vorticity is generated and evolves, which is necessary for understanding, and thus modeling, the fundamental physics of circulation in the nearshore coastal ocean.

Data Availability Statement

The current meter data from the ring and the high-spatial resolution survey can be found here: https://doi.org/10.17603/ds2-c9p4-7264 (Elgar & Raubenheimer, 2019). The other surveys and offshore wave conditions can be found on the FRF THREDDS server: https://chlthredds.erdc.dren.mil/thredds/catalog/frf/catalog.html. The remote sensing data are available at: https://doi.org/10.5281/zenodo.11581091 (Dooley, Elgar, & Raubenheimer, 2024).

Acknowledgments
We thank the field crews of the PVLAB and the FRF for obtaining observations in often difficult surfzone conditions, and Drs. David Clark and Jeff Hansen for their roles in the 2013 field project. Funding was provided by the National Science Foundation, a Vannevar Bush Faculty Fellowship, a National Defense Science and Engineering Graduate Fellowship, the US Coastal Research Program, a Woods Hole Oceanographic Independent Study Award, and the Ocean Ventures Fund.

References

Baker, C., Moulton, M., Chickadel, C., Nuss, E., Palmsten, M., & Brodie, K. (2023). Two-dimensional inverse energy cascade in a laboratory surf zone for varying wave directional spread. *Physics of Fluids*, *35*(12). https://doi.org/10.1063/5.0169895

Baker, C., Moulton, M., Raubenheimer, B., Elgar, S., & Kumar, N. (2021). Modeled three-dimensional currents and eddies on an alongshore-variable barred beach. *Journal of Geophysical Research: Oceans*, *126*(7), e2020JC016899. https://doi.org/10.1029/2020JC016899

Boehm, A. B. (2003). Model of microbial transport and inactivation in the surf zone and application to field measurements of total coliform in Northern Orange County, California. *Environmental Science and Technology*, *37*(24), 5511–5517. https://doi.org/10.1021/es034321x

Boehm, A. B., Ismail, N. S., Sassoubre, L. M., & Andruszkiewicz, E. A. (2017). Oceans in peril: Grand challenges in applied water quality research for the 21st century. *Environmental Engineering Science*, *34*(1), 3–15. https://doi.org/10.1089/ees.2015.0252

Bonneton, P., Bruneau, N., Castelle, B., & Marche, F. (2010). Large-scale vorticity generation due to dissipating waves in the surf zone. *Discrete and Continuous Dynamical Systems – B*, *13*(4), 729–738. https://doi.org/10.3934/dcdsb.2010.13.729

Brown, J. A., MacMahan, J. H., Reniers, A. J. H. M., Thornton, E. B., Shanks, A. L., Morgan, S. G., & Gallagher, E. L. (2019). Observations of mixing and transport on a steep beach. *Continental Shelf Research*, *178*, 1–14. https://doi.org/10.1016/j.csr.2019.03.009

Bruneau, N., Bonneton, P., Castelle, B., & Pedreros, R. (2011). Modeling rip current circulations and vorticity in a high-energy mesotidal-macrotidal environment. *Journal of Geophysical Research*, *116*(C7), 2010JC006693. https://doi.org/10.1029/2010JC006693

Bühler, O. (2000). On the vorticity transport due to dissipating or breaking waves in shallow-water flow. *Journal of Fluid Mechanics*, *407*, 235–263. https://doi.org/10.1017/S0022112099007508

Bühler, O., & Jacobson, T. E. (2001). Wave-driven currents and vortex dynamics on barred beaches. *Journal of Fluid Mechanics*, *449*, 313–339. https://doi.org/10.1017/S0022112001006322

Chen, J., Raubenheimer, B., & Elgar, S. (2024). Wave and roller transformation over barred bathymetry. *Journal of Geophysical Research: Oceans*, *129*(5), e2023JC020413. https://doi.org/10.1029/2023JC020413

Clark, D. B., Elgar, S., & Raubenheimer, B. (2012). Vorticity generation by short-crested wave breaking. *Geophysical Research Letters*, *39*(24), 2012GL054034. https://doi.org/10.1029/2012GL054034

Clark, D. B., Feddersen, F., & Guza, R. T. (2010). Cross-shore surfzone tracer dispersion in an alongshore current. *Journal of Geophysical Research*, *115*(C10), 2009JC005683. https://doi.org/10.1029/2009JC005683

Dalrymple, R., MacMahan, J., Reniers, A., & Nelko, V. (2011). Rip currents. *Annual Review of Fluid Mechanics*, *43*(1), 551–581. https://doi.org/10.1146/annurev-fluid-122109-160733

Dooley, C., Elgar, S., & Raubenheimer, B. (2024). PVLAB: Remotely sensed surface currents from field experiments (2013, 2018, 2021, 2022) [Dataset]. Zenodo. https://doi.org/10.5281/zenodo.11581091

Dooley, C., Elgar, S., Raubenheimer, B., & Gorrell, L. (2024). Estimating surfzone currents with near-field optical remote sensing. *Journal of Atmospheric and Oceanic Technology*. sub judice.

Elgar, S., Dooley, C., Gorrell, L., & Raubenheimer, B. (2023). Observations of two-dimensional turbulence in the surfzone. *Physics of Fluids*, *35*(8), 085142. https://doi.org/10.1063/5.0159170

Elgar, S., & Raubenheimer, B. (2019). Surfzone vorticity and advection (RODSEX) field experiment [Dataset].DesignSafe-CI. https://doi.org/10.17603/ds2-c9p4-7264

Elgar, S., & Raubenheimer, B. (2020). Field evidence of inverse energy cascades in the surfzone. *Journal of Physical Oceanography*, *50*(8), 2315–2321. https://doi.org/10.1175/JPO-D-19-0327.1

Feddersen, F. (2007). Breaking wave induced cross-shore tracer dispersion in the surf zone: Model results and scalings. *Journal of Geophysical Research*, *112*(C9), 2006JC004006. https://doi.org/10.1029/2006JC004006

Feddersen, F., Boehm, A. B., Giddings, S. N., Wu, X., & Liden, D. (2021). Modeling untreated wastewater evolution and swimmer illness for four wastewater infrastructure scenarios in the San Diego-Tijuana (US/MX) border region. *GeoHealth*, *5*(11), e2021GH000490. https://doi.org/10.1029/2021GH000490

Feddersen, F., Clark, D. B., & Guza, R. T. (2011). Modeling surf zone tracer plumes: 1. Waves, mean currents, and low-frequency eddies. *Journal of Geophysical Research*, *116*(C11), 2011JC007210. https://doi.org/10.1029/2011JC007210

Geiman, J. D., & Kirby, J. T. (2013). Unforced oscillation of rip-current vortex cells. *Journal of Physical Oceanography*, *43*(3), 477–497. https://doi.org/10.1175/JPO-D-11-0164.1

Grant, S. B., Kim, J. H., Jones, B. H., Jenkins, S. A., Wasyl, J., & Cudaback, C. (2005). Surf zone entrainment, along-shore transport, and human health implications of pollution from tidal outlets. *Journal of Geophysical Research*, *110*(C10025), 20. https://doi.org/10.1029/2004JC002401

Grimes, D., & Feddersen, F. (2021). The self-similar stratified inner-shelf response to transient rip-current-induced mixing. *Journal of Fluid Mechanics*, *915*, A82. https://doi.org/10.1017/jfm.2021.140

Haas, K., Svendsen, I., HallerZhao, M. Q., & Zhao, Q. (2003). Quasi-three-dimensional modeling of rip-current systems. *Journal of Geophysical Research*, *108*(C7), 3217. https://doi.org/10.1029/2002JC001355

19448007, 2024, 20, Downloaded from https://agupubs.onlinelibrary.wiley.com/doi/10.1029/2024GL111402 by Ciara Dooley - Mbl Whoi Library , Wiley Online Library on [24/10/2024]. See the Terms and Conditions (https://onlinelibrary.wiley.com/terms-and-conditions) on Wiley Online Library for rules of use; OA articles are governed by the applicable Creative Commons License

Hally-Rosendahl, K., & Feddersen, F. (2016). Modeling surfzone to inner-shelf tracer exchange. *Journal of Geophysical Research: Oceans*, *121*(6), 4007–4025. https://doi.org/10.1002/2015JC011530

Hally-Rosendahl, K., Feddersen, F., Clark, D. B., & Guza, R. T. (2015). Surfzone to inner-shelf exchange estimated from dye tracer balances. *Journal of Geophysical Research: Oceans*, *120*(9), 6289–6308. https://doi.org/10.1002/2015JC010844

Hally-Rosendahl, K., Feddersen, F., & Guza, R. T. (2014). Cross-shore tracer exchange between the surfzone and inner-shelf. *Journal of Geophysical Research: Oceans*, *119*(7), 4367–4388. https://doi.org/10.1002/2013JC009722

Johnson, D., & Pattiaratchi, C. (2006). Boussinesq modelling of transient rip currents. *Coastal Engineering*, *53*(5–6), 419–439. https://doi.org/10.1016/j.coastaleng.2005.11.005

Kennedy, A. B., Brocchini, M., Soldini, L., & Gutierrez, E. (2006). Topographically controlled, breaking-wave-induced macrovortices. Part 2. Changing geometries. *Journal of Fluid Mechanics*, *559*, 57. https://doi.org/10.1017/S0022112006009979

Kumar, N., & Feddersen, F. (2017). A new offshore transport mechanism for shoreline-released tracer induced by transient rip currents and stratification. *Geophysical Research Letters*, *44*(6), 2843–2851. https://doi.org/10.1002/2017GL072611

Morgan, S. G., Shanks, A. L., MacMahan, J. H., Reniers, A. J. H. M., & Feddersen, F. (2018). Planktonic subsidies to surf-zone and intertidal communities. *Annual Review of Marine Science*, *10*(1), 345–369. https://doi.org/10.1146/annurev-marine-010816-060514

Moulton, M., Suanda, S. H., Garwood, J. C., Kumar, N., Fewings, M. R., & Pringle, J. M. (2023). Exchange of plankton, pollutants, and particles across the nearshore region. *Annual Review of Marine Science*, *15*(1), 167–202. https://doi.org/10.1146/annurev-marine-032122-115057

O'Dea, A., Kumar, N., & Haller, M. C. (2021). Simulations of the surf zone eddy field and cross-shore exchange on a nonidealized bathymetry. *Journal of Geophysical Research: Oceans*, *126*(5). https://doi.org/10.1029/2020JC016619

Peregrine, D. H. (1998). Surf zone currents. *Theoretical and Computational Fluid Dynamics*, *10*(1), 295–309. https://doi.org/10.1007/s001620050065

Peregrine, D. H. (1999). Large-scale vorticity generation by breakers in shallow and deep water. *European Journal of Mechanics - B: Fluids*, *18*(3), 403–408. https://doi.org/10.1016/S0997-7546(99)80037-5

Salatin, R., Chen, Q., Raubenheimer, B., Elgar, S., Gorrell, L., & Li, X. (2024). A new framework for quantifying alongshore variability of swash motion using fully convolutional networks. *Coastal Engineering*, *192*, 104542. https://doi.org/10.1016/j.coastaleng.2024.104542

Spydell, M., & Feddersen, F. (2009). Lagrangian drifter dispersion in the surf zone: Directionally spread, normally Incident waves. *Journal of Physical Oceanography*, *39*(4), 809–830. https://doi.org/10.1175/2008JPO3892.1

Spydell, M., Feddersen, F., & Guza, R. (2009). Observations of drifter dispersion in the surfzone: The effect of sheared alongshore currents. *Journal of Geophysical Research*, *114*(C7), 2009JC005328. https://doi.org/10.1029/2009JC005328

Straub, J., Cialone, M., Raubenheimer, B., Brown, J., Elko, N., & Brodie, K. (2023). The during nearshore event experiment (DUNEX): A collaborative coastal community experiment to address coastal resilience. *Shore and Beach*, 23–29. https://doi.org/10.34237/1009133

Suanda, S., & Feddersen, F. (2015). A self-similar scaling for cross-shelf exchange driven by transient rip currents. *Geophysical Research Letters*, *42*(13), 5427–5434. https://doi.org/10.1002/2015GL063944

Thomson, S. W. (1910). *Mathematical and physical papers: Vol. IV. Hydrodynamics and general dynamics*. Cambridge University Press.

Wei, Z., Dalrymple, R. A., Xu, M., Garnier, R., & Derakhti, M. (2017). Short-crested waves in the surf zone. *Journal of Geophysical Research: Oceans*, *122*(5), 4143–4162. https://doi.org/10.1002/2016JC012485

Wu, X., Feddersen, F., & Giddings, S. N. (2021). Diagnosing surfzone impacts on inner-shelf flow spatial variability using realistic model experiments with and without surface gravity waves. *Journal of Physical Oceanography*, *51*(8), 2505–2515. https://doi.org/10.1175/JPO-D-20-0324.1

19448007, 2024, 20, Downloaded from https://agupubs.onlinelibrary.wiley.com/doi/10.1029/2024GL111402 by Ciara Dooley - Mbl Whoi Library , Wiley Online Library on [24/10/2024]. See the Terms and Conditions (https://onlinelibrary.wiley.com/terms-and-conditions) on Wiley Online Library for rules of use; OA articles are governed by the applicable Creative Commons License